IEEE Access
Multidisciplinary ⋮ Rapid Review ⋮ Open Access Journal

Received 21 June 2023, accepted 14 July 2023, date of publication 18 July 2023, date of current version 24 July 2023.

*Digital Object Identifier 10.1109/ACCESS.2023.3296459*

RESEARCH ARTICLE

# Adaptive Antenna Impedance Matching Using Low-Complexity Shallow Learning Model

**MOHAMMAD MAHMUDUL HASAN AND MICHAEL CHEFFENA**
Faculty of Engineering, Norwegian University of Science and Technology (NTNU), 2815 Gjøvik, Norway
Corresponding author: Mohammad Mahmudul Hasan (mohammad.m.hasan@ntnu.no)

This work was supported by the Research Council of Norway under Project 324061.

**ABSTRACT** In this paper, an automatic antenna impedance matching technique is presented for a wide range of frequency bands where a low-complexity shallow learning model adaptively determines the component values of the matching circuit on a real-time. In general, matching networks require both the real and imaginary parts of the antenna impedance to determine the tuning parameters which involves expensive measurement equipment. The shallow learning model developed in this work needs only the magnitude of the antenna reflection coefficients ($S_{11}$) to construct the impedance matching circuit. First, the tuning parameters were theoretically calculated and used for computer simulations to generate the $S_{11}$ data. In total 500 samples were generated, of which, 400 were used for training and 100 for validation. The proposed technique was applied to a novel inverted-F antenna resonating at 2.45 GHz for impedance matching. The achieved results show stable performances over a wide range of frequencies from 2 to 3 GHz. For validation, the performances of the impedance matching circuit were simulated using predicted and calculated tuning parameters. Results confirm comparable performances in terms of the antenna's resonance frequency, reflection coefficients, and operational 10-dB bandwidth. The fast prediction ability of the proposed low complexity shallow learning model makes it suitable for real-time applications. Moreover, repeated $K$-fold cross validation confirms a stable 0.99985 accuracy of the proposed model when repeated 15 times.

**INDEX TERMS** Antenna impedance matching, impedance mismatch, antenna sensors, shallow learning model, inverted-F antenna.

## I. INTRODUCTION

Antennas used in wireless communications are one of the key elements that greatly determine the overall performance of the system. Wireless applications in general require their antennas to resonate within fixed band(s) of operating frequency. These antennas are also designed to be impedance matched with the radio frequency (RF) front-end. A properly matched antenna section, i.e., when the antenna is at a resonance, maximum power transmission, maximum coverage, reduced power consumption, high signal-to-noise ratio, and stable communication can be ensured [1], [2]. However, antennas in electronic devices can be detuned (deviated from designed resonance frequency) by several random factors. In handheld devices, for example, when a user receives a phone call, the hand movement and the user proximity create an impedance mismatch. When a call is in progress, the phone is held very near to the user's ear (and head). This interaction between the antenna and the person's head, that acts as a lossy dielectric, further causes impedance mismatch [3], [4], [5]. The effect of the textile on the human body, its thickness, air gap between textile and skin can also contribute to antenna impedance mismatch. This greatly reduces antenna radiation efficiency, transmission range, and overall performances [1], [3], [4], [5], [6], [7]. Recently, sensor antennas are becoming more and more prevalent due to their dual functionality i.e., simultaneous sensing and communicating capability [8], [9], [10], [11], [12]. When sensor antennas are openly placed in the sensing environment in contact with the target analyte (in the form liquid, solid or gas), sensing is usually done by changing the resonant frequency of the antenna which can affect its communication performance.

The associate editor coordinating the review of this manuscript and approving it for publication was Jose Saldana.

To ensure antenna's dual functionality (i.e., sensing and communications), a real-time adaptive and automatic impedance matching system becomes important. Several decades of extensive research on this topic revealed numerous effective solutions to this problem that falls mostly under two major categories: Reconfigurable Antenna (RA) and Antenna Impedance Matching (AIM) circuit. RAs can achieve frequency adjustment, change in the radiation patterns, polarization, etc., by changing its electrical configuration through switches. A solid-state plasma chip antenna with a surface positive-intrinsic-negative (PIN) diode is proposed in [13] that can achieve reconfigurability. Additional switches were used to toggle between sensing and communication modes, and three varactor diodes to tune the operating frequencies and achieved good radiation performances, however, with high complexity [14]. Varactor diodes can tune both the resonance frequency and polarization of the antenna by varying the voltage applied to the varactors [15]. Varactor diodes can also be used in a wideband compact loop antenna for 0.9, 2.4, 3.5, and 5.5 GHz applications where each of these bands can be tuned separately [16]. Recently, water-based antenna has drawn attention due to its low cost and ease of reconfigurability [17]. Here, the operating frequency can be tuned by controlling the filling status of water. Different shapes and thickness of layers can achieve continuous tuning of the resonance frequency ranging from 1.1 to 2.2 GHz [17]. However, electrically RAs involve complicated design, complex structure and require complex biasing systems making them less attractive for next general of wireless communication that require low-complex circuitry for high-speed operation [18], [19].

On the other hand, AIM circuits are directly placed between the transceiver and antenna with no electrical (or physical) reconfiguration to the antenna [20], [21], [22], [23], [24], [25], [26], [27], [28], [29], [30], [31], [32], [33], [34], [35], [36], [37]. Antenna's resonating frequency is then adjusted by changing component values of the AIM circuit, making them easy to implement. The first challenge is that these circuits are desired to be adaptive and automatic for real-time applications. For fixed inductor and capacitor values, the circuit resonates at a single frequency, thus, not suitable to track and compensate for the changes in antenna's operational condition. Additionally, today's battery-operated wireless devices need on-chip antenna tuning with low-complex circuitry for high-speed operation and low-power consumption. Such solutions are, however, still challenging. The second challenge is that the design of AIM circuits in general requires accurate measurement of the complex impedance of the antenna. Several techniques are available to measure this such as quadrature detectors [20], and RF peak detectors [21]. A combination of capacitors with planner inverted-F antenna can achieve a wide frequency tuning range that covers from 2 to 4 GHz [22]. Channel capacity metric can be used as a guideline to design an AIM circuit [23]. Additional sensory circuit can be used to monitor the fluctuations in the AIM circuit, where control-loops are used to independently control the real and imaginary parts of the impedance [24]. However, these complex measurement techniques make them less attractive for battery driven applications such as handheld devices. Optimization techniques can also tune an LC-network iteratively until the matching component values are found, and the impedance matching goal is met. These traditional techniques, however, are based on iterative algorithms, thus, not fast enough for real-time impedance matching. Gradient algorithms are computationally expensive and often converge to a local optimum [25]. Non-gradient based optimization techniques, such as genetic algorithms are also available, with some limitations such as large storage, loss of best chromosome, premature convergence, local optimum during evolution [26], [27], [28], [29], [30]. Later, fuzzy inference system was found to be 80.26% more efficient than genetic algorithms [31]. Quantum inspired genetic algorithms have shown to overcome the limitations of conventional genetic algorithms by factoring or searching in an unstructured database. Results also confirm the feasibility for real-time application in RF-front-end systems. Furthermore, software defined solutions can ensure automatic tuning [32], [33].

Recently, machine learning received huge attention for solving antenna optimization problems [34], [35], [36], [37], [38]. For example, Deep Neural Network (DNN) was used for shape optimization and the location of antenna feeding point in [34]. Later, DNN was used to determine optimal design parameters of the bent wire antenna [35]. A feedforward-backpropagation neural network is presented in [36] to design impedance matching circuit for wireless power transmission with good efficiency, however, with limited range of impedance. A range-adaptive solution based on neural network achieved 90% wireless power transfer (WPT) efficiency in [37]. However, the techniques proposed in [36] and [37] are applicable for WPT only and suitable for low frequency applications. These solutions cannot tune antenna impedances for wireless applications. Recently, DNN was used to construct tuneable matching circuit for wireless applications using only the magnitude of the Return Loss (RL) [38]. The authors used 377 simulated training samples for a frequency range from 0.8 to 1.5 GHz to train a DNN. However, the complex structure of DNN is not fast enough to track the dynamic nature of today's wireless environment. The proposed DNN model in [38] required 10.5 minutes using Intel(R) Xenon(R) processor at 2.30 GHz and 16 GB memory. Clearly, the time complexity of [38] is not suitable for real-time applications. To date, only neural networks have been used for impedance matching. The contribution of our work can be summarised as:

- For the first time we propose a Shallow Learning Model (SLM) with no hidden layers to construct an AIM circuit that requires 0.05 seconds (50ms) for the training, and only 0.001 second (1ms) to make a prediction, unlike the previous DNN based solution that required 10.5 minutes [38].

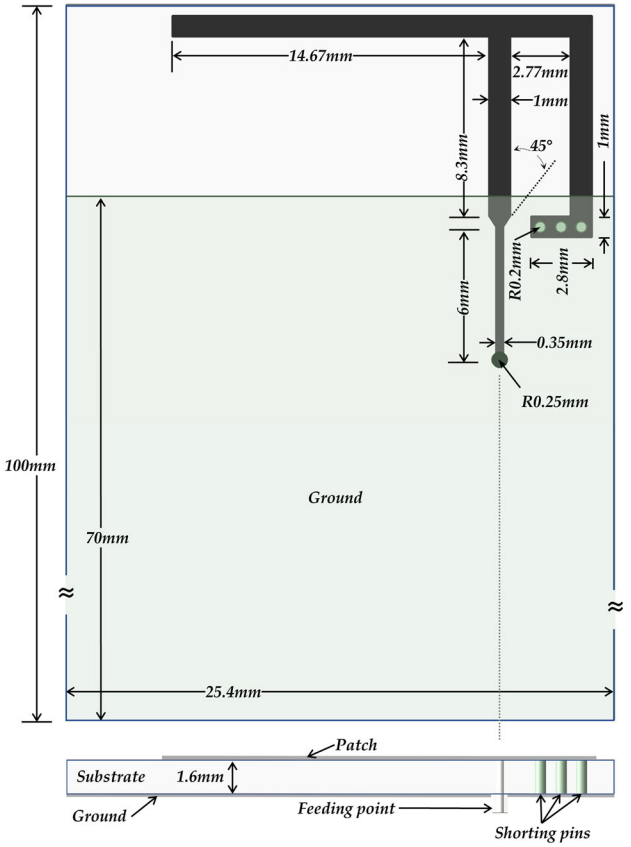


**FIGURE 1.** Inverted-F antenna used for impedance matching.

- Unlike previous works where arbitrarily values of matching circuit components were considered, we used interpolated tuning values to reduce the training time and improve the training accuracy. Accurate measurement of complex impedances requires expensive equipment such as a vector-network-analyser or spectrum analyser. Through training, the proposed shallow learning model can learn to find the complex impedances entirely from the magnitude of the $S_{11}$ data without needing to calculate the real or imaginary values of the impedance. Data analysis also shows that a proper dimensionality reduction can further reduce the model's complexity.

The remaining of this paper is organized as follows. Section II presents a novel antenna design to generate $S_{11}$ data and evaluate performances of proposed impedance matching technique. A step-by-step development of the impedance matching circuit is presented in Section III. Section IV explains the datasets used in this work. In Section V, we develop a low-complexity machine learning model using a shallow learning approach. Section VI discusses the findings and obtained results.

## II. INVERTED-F ANTENNA STRUCTURE

The aim of this work is to develop a machine learning model that learns from the changes in the antenna's operational conditions and adapts itself to these changes for impedance matching by tuning the circuit parameters. To track these variations and evaluate the performances, we designed a novel inverted-F antenna structure as shown in Fig. 1 for wireless hand-held applications (where the RF section is most likely to face the maximum impedance variation). We used this antenna to generate the required magnitude of the RL ($S_{11}$) for the model training, and to evaluate the performances of impedance matching circuit. Inverted-F antenna structures are widely used as primary antennas for mobile devices due to their radiation efficiency, wideband, and miniaturized size. These are low-profile, quarter-wave short-circuit monopole antennas where an inverted-F shaped patch is placed in parallel to the ground plane with an inductively tuned stub in parallel with the capacitive radiating arm. Monopole antennas are usually capacitive in nature, however, placing a shorting stub increases inductance to achieve impedance matching. In this work, the antenna is designed to achieve an exact resonance at 2.45 GHz on an air substrate layer and thickness of 1.6 mm. The antenna has a length of 19.44 mm and a height of 1.6 mm from the ground. The width of the patch element throughout the structure is 1.0 mm. The shorting stub, 2.77 mm away from the feeding arm, is connected to the ground with three shorting pins of solid copper contact of 0.2 mm radius each. The matching circuit is placed with the feeding point. We simulated the antenna structure using Ansys HFSS (high frequency electromagnetic simulation software). The RL in Fig. 2(a) shows that the designed antenna is perfectly matched (without the matching circuit) at 2.45 GHz with a 200 MHz of bandwidth. The Voltage Standing Wave Ratio (VSWR), in Fig. 2(b), is 1.0 (which is ideally minimum) at 2.45 GHz. This also confirms impedance matching and absolutely no power is reflected from the antenna. One of the many advantages an Inverted-F antenna can offer is that it can be made meandered to house in a narrow space of handheld devices and yet can achieve a high bandwidth. The magnitude of the complex antenna impedance ($Z_{11}$) along with its real and imaginary parts are given in Fig. 2(c). This shows that the impedance is purely real at the resonating frequency. A smith chart in Fig. 2(d) graphically represents the location of the complex impedances for the total frequency range. Using a coaxial cable transmission line with a 50 Ω input impedance, Fig. 2(d) confirms that the designed antenna is normalized at 2.45 GHz. The complex impedances of frequencies higher than 2.45 GHz are located on the upper inductive part and for the frequencies lower than 2.45 GHz are located on the lower capacitive part of the smith chart.

## III. ANTENNA IMPEDANCE MATCHING (AIM) CIRCUIT

The development of an AIM circuit is illustrated in Fig. 3. As shown in Fig. 3(a), a parallel capacitor ($C_p$) first moves complex impedance from both the inductive (BC arc) and capacitive parts (AB arc) along the conductance circles to a single unit resistance circle, on BD arc. Then, a series inductor ($L_s$) moves the impedance along the unit resistance circle to the target point (B). Fig. 2(c) confirmed that all

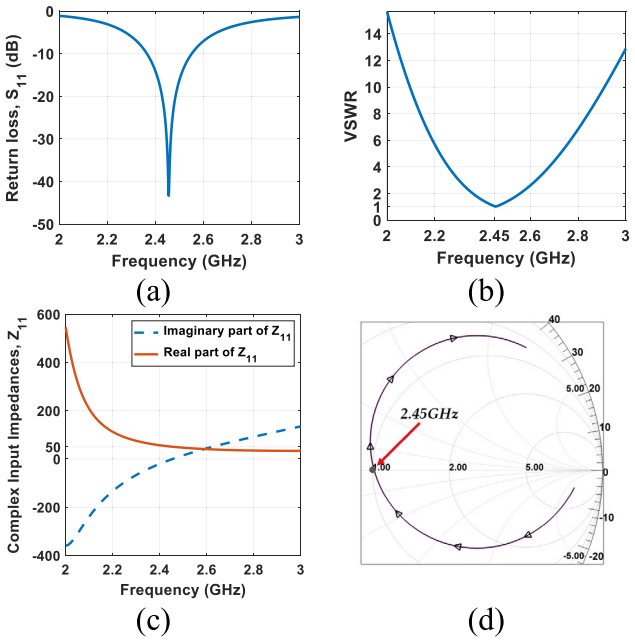


**FIGURE 2.** Simulation of the proposed inverted-F antenna: (a) RL ($S_{11}$); (b) VSWR; (c) Complex input impedance $Z_{11}$; (d) Smith chart.

the impedances are in the permissible region of an $L$-type $LC$-network, thus, such a single network can be constructed with an inductor in series and a capacitor in parallel to tune all the impedance points without entering the forbidden region of the circuit. Then, the inductor and capacitor can be tuned to match over the target range of frequencies. The proposed $L$-type $LC$-network is shown in Fig. 3(b). $Z_S$, is the source impedance, $Z_L$ is the load impedance. $Z_m$ and $Z_i$ represent impedance transformations after each stage from load-to-source during impedance matching, respectively. For a purely resistive source, the impedance of the matching network needs to be complex conjugate of the load impedance. To transfer maximum real power to the load, i.e., achieve impedance matching, $Z_i$ must equal the source impedance, $Z_s$. From Fig. 3(b), we obtain,

$$Z_m = \frac{Z_L}{1 + j\omega C_p Z_L}, \tag{1}$$

where $Z_L = R_L + jX_L$, and $\omega$ is the angular frequency. Letting $Z_m = R_m + jX_m$, we get

$$R_m = \frac{R_L}{\left(\omega C_p R_L\right)^2 + \left(1 - \omega C_p X_L\right)^2}, \tag{2}$$

and

$$X_m = \frac{X_L - \omega C_p \left(R_L^2 + X_L^2\right)}{\left(\omega C_p R_L\right)^2 + \left(1 - \omega C_p X_L\right)^2}. \tag{3}$$

Finally, we get the input impedance as,

$$Z_i = Z_m + j\omega L_s = R_m + j\left(X_m + \omega L_s\right). \tag{4}$$

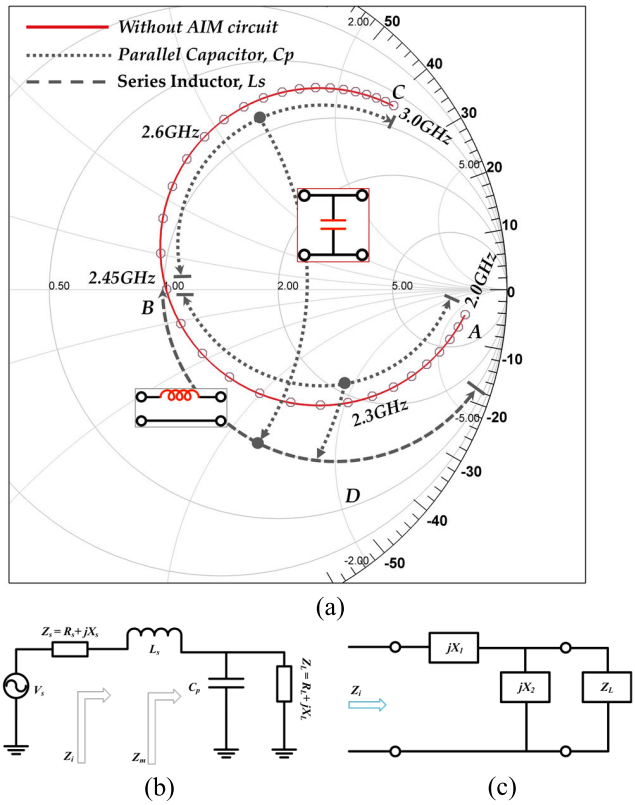


**FIGURE 3.** Step-by-step development of AIM circuit. (a) Movement of impedances using parallel capacitor and series inductor. (b) L-type *LC*-network for AIM circuit; (c) Simplified circuit.

Denoting $Z_i = R_i + jX_i$ and equating real and complex terms separately, we get,

$$R_i = \frac{R_L}{\left(\omega C_p R_L\right)^2 + \left(1 - \omega C_p X_L\right)^2}, \tag{5}$$

and

$$X_i = \frac{X_L - \omega C_p \left(R_L^2 + X_L^2\right)}{\left(\omega C_p R_L\right)^2 + \left(1 - \omega C_p X_L\right)^2} + \omega L_s. \tag{6}$$

From (4), we can calculate reflection-coefficient at the input of AIM circuit as,

$$\Gamma_{in} = \frac{Z_i - Z_s}{Z_i + Z_s}, \tag{7}$$

and VSWR as

$$VSWR = \frac{1 + |\Gamma_{in}|}{1 - |\Gamma_{in}|}. \tag{8}$$

To determine the tuning parameters, a simplified structure of Fig. 3(b) is given in Fig. 3(c). To achieve impedance matching, $Z_i$ must equal to the characteristic impedance of the transmission line, $Z_0$. From Fig. 3(c),

$$Z_0 = jX_1 + \left(jX_2 + \frac{1}{Z_L}\right)^{-1} = jX_1 + \frac{R_L + jX_L}{jX_2 R_L - X_2 X_L + 1}. \tag{9}$$

**TABLE 1. Calculated values of tuning parameters.**

| Frequency (GHz) | Capacitor value, $C_p$ (fF) | Inductor value, $L_s$ (nH) |
|---|---|---|
| 2.0 | 324.91 | 15.20 |
| 2.2 | 246.70 | 7.60 |
| 2.4 | 183.65 | 1.75 |
| 2.6 | 1360.00 | 2.69 |
| 2.8 | 977.98 | 6.04 |
| 3.0 | 670.07 | 8.59 |

Simplifying (9) and equating the real and imaginary terms on both sides we get

$$X_2 (R_L X_1 - Z_0 X_L) = R_L - Z_0, \tag{10}$$

and

$$X_1 (1 - X_2 X_L) = X_2 Z_0 R_L - X_L. \tag{11}$$

Solving (10) and (11), we get

$$X_1 = \frac{X_2 Z_0 R_L - X_L}{1 - X_2 X_L}. \tag{12}$$

and

$$X_2 = \frac{X_L \pm \sqrt{\frac{R_L}{Z_0}(R_L^2 + X_L^2 - Z_0 R_L)}}{R_L^2 + X_L^2}. \tag{13}$$

Two solutions for $X_2$ are possible from (13), and both can be used for implementation. The proposed $L$-type $LC$ network provides required tuning parameters to cover entire range of frequency over 2 to 3 GHz to achieve an ideal impedance matching ($\Gamma_{in} = 0$ and VSWR = 1). Six sets of $LC$ values were determined using (12) and (13) (see Table 1). At 2.0 GHz, for example, the matching parameters are $C_p = 0.32491$ pF and $L_s = 15.21$ nH, respectively. At 3.0 GHz, the values are $C_p = 0.67007$ pF and $L_s = 8.59$ nH, respectively.

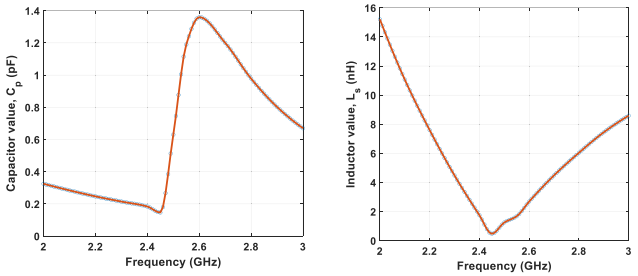


(a) (b)

**FIGURE 4. (a) Interpolation of data using piecewise cubic Hermite Interpolating Polynomial algorithm for (a) parallel capacitor, $C_p$ and (b) series inductor, $L_s$.**

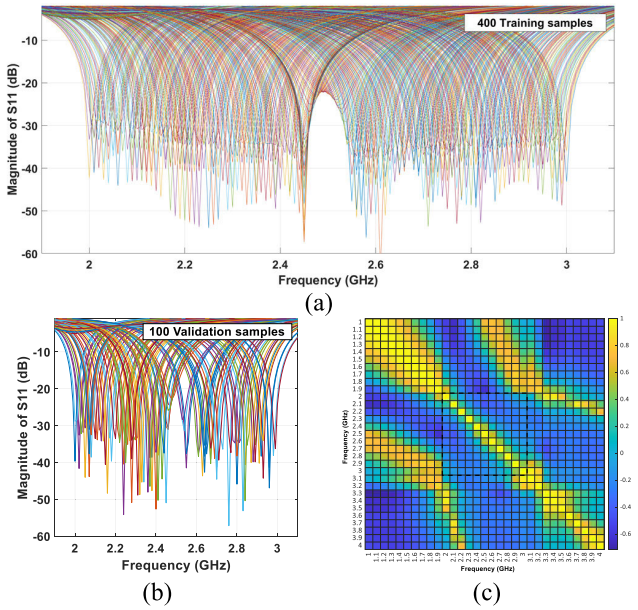


(a) (b) (c)

**FIGURE 5. (a) Simulated values of $S_{11}$: (a) 400 samples for training (b) 100 samples for validation (c) Heatmap of the correlation matrix of $S_{11}$.**

## IV. DATASET PREPARATION

Accurate measurement of antenna impedance, including real and imaginary parts, is essential to construct a tuning circuit and achieve impedance matching. This is possible to measure, however, it requires expensive equipment such as a vector network-analyser. A larger dataset is also required for effective training of machine learning models and accurate prediction of the circuit parameters. To manually produce such a large dataset using commercial network-analysers would be a time consuming and cumbersome task. Instead, we developed a programming-interface, using IronPython, that interconnects antenna simulation software and Python. To obtain the required $S_{11}$ dataset, we generated synthetic data to simulate the inverted-F antenna. We used piecewise cubic polynomial interpolation on mathematically obtained datasets (see Table 1), unlike previous works [38] where linear values were considered. This further improves the training accuracy during simulation. Cubic Hermite polynomial uses the current shape of the given data points and produces additional interpolation points [39]. Interpolation in general defines a function that estimates unknown values from given data points. A piecewise cubic Hermite interpolator uses monotonic cubic splines to preserve the overall shape in the given dataset and it does not overshoot or undershoot during interpolation. We produced 500 interpolation points for the tuning parameters using shape preserving interpolation technique given in [40] and shown in Fig. 4. The programming-interface selects a pair of tuning parameters each time, simulates the inverted-F antenna in HFSS, and a total of 500 $S_{11}$ results are obtained in the form of comma-separated value (csv) file. Each of which contains 300 data points corresponding to the frequency range from 2 to 3 GHz. Fig. 5(a) shows 400 samples of $S_{11}$ results that were used for the training, and Fig. 5(b) shows the remaining 100 samples used for the validation.

During data analysis, we also noticed the presence of multicollinearities in the dataset, i.e., two or more input

**TABLE 2. Algorithm for impedance matching using SLM.**

| **Algorithm** SLM based Impedance Matching Network | |
|---|---|
| Procedure SLM_NETWORK ($\|S_{11}\|$, $\alpha$) | |
| **1** | **start** |
| **2** | measure $\|S_{11}\|$ |
| **3** | **if** $S_{11} \leq$ -10 dB |
| **4** | **goto** step 2 |
| **5** | **else** |
| | apply $\|S_{11}\|$ data to the input layer: SLM[$\|S_{11}\|, \alpha$]. output layer computes (14), (15) and obtain $[C_p, L_s] = f_k(\mathbf{x})_{k=1,2}$ from output layer. |
| **8** | tune AIM circuit with obtained $C_p$, $L_s$ in **8** |
| **9** | **then goto** step **2** |
| **10** | **end procedure** |

features are highly (or almost linearly) correlated. Fig. 5(c) shows a heatmap of the correlation matrix of the feature dataset where several $S_{11}$ results are correlated with several adjacent frequency points. $S_{11}$ curves, in general, including multiband or wideband antennas, will have a specific number of minimums to specific frequencies and few sidebands. It is, however, possible to consider the range of target frequency, i.e., 2 to 3 GHz. Instead, we considered the entire range of frequency (1 to 4 GHz) to consider the sidebands during training and improve the prediction accuracy further. Simultaneously, proper techniques must be used during data processing to avoid high dimensional computational complexity. A learning algorithm in general finds correlation between the input features and the target variable(s) to learn from patterns. In this work, a learning algorithm learns solely from $S_{11}$ magnitude, thus, a high level of multicollinearities between input features can produce misleading outcomes. Without addressing the presence of multicollinearities in the dataset, learning algorithms can make poor (or wrong) predictions. A straightforward solution is to remove correlated features and train the model from the rest. This only reduces the model's predictabilities at these frequencies.

## V. MACHINE LEARNING MODEL: SHALLOW APPROACH

In this work, we use $S_{11}$ data to train a shallow learning model which then can determine tuning circuit parameters to achieve impedance matching automatically. Machine learning algorithms learn from the hidden patterns present in the dataset and become capable of predicting unseen data. In general, shallow learning models are machine learning models where complex structures of deep layered-neural network or multilayer perceptron are not involved. In this work, we used a low complexity, yet efficient algorithm for impedance matching given in Table 2. We used Sci-kit's python class for shallow learning model and its parameterized grid search for optimal hyperparameter search. Sci-kit's pipeline encapsulates data pre-processing, transformations, and a final estimating model. This builds a model that improves the algorithm's accuracy. We used ridge regression as estimator to reduce collinearities from dataset. Ridge regularization works by adding a penalty, equal to the square of the coefficient, to the cost function which shrinks ridge coefficients. In general, for a given set of $N$ data points $(\mathbf{x}_i, \mathbf{y}_i)_{i=1}^{N}$, the ridge estimator finds a function, $f(\mathbf{x})$ as

$$f(\mathbf{x}) = \mathbf{x}^{\mathrm{T}}\mathbf{w} = \sum_{j=1}^{M} x_j w_j \tag{14}$$

by setting parameters $\mathbf{w} = (w_1, \cdots, w_M)^T$ in such a way so that $f(\mathbf{x})$ approximates $y_i$ as much as possible. Then, the estimator minimizes the sum of squared residuals plus a regularization term and has the optimal fitting parameters,

$$\mathbf{w} = \underset{\mathbf{w}}{\operatorname{argmin}} \sum_{i=1}^{N} |f(\mathbf{x}_i) - y_i|^2 + \alpha \|\mathbf{w}\|^2 \tag{15}$$

where $\|\mathbf{w}\|$ is the 2-norm of $\mathbf{w}$. In our case, the algorithm estimates two separate outputs as $f_k(\mathbf{x})_{k=1,2} = \mathbf{x}^{\mathrm{T}}\mathbf{w}_{k=1,2}$. The controlling parameter, alpha ($\alpha$), in (15) adds a constraint to the coefficients as a penalty factor to control the amount of shrinkage. For $\alpha > 0$, this causes the ridge coefficients to tend towards zero, but neither setting them zero nor removing them as each of the $S_{11}$ results corresponds to specific tuning elements. The larger the value of the constraint, the more robust it becomes against multicollinearities in the dataset. Initial pre-processing involved data scaling (to make the mean $= 0$ and standard deviation $= 1.0$) as ridge estimators are extremely sensitive to input data scale.

As observed from the heatmap of $S_{11}$ correlation matrix in Fig. 5(c), several columns appeared to be strongly correlated (more than 0.9 correlation). This is because most of the data points in $S_{11}$ curves will be constant except one minimum (or more for multiband antenna) pointing the resonance frequency (or frequencies). If there are two (or more) features that show such degree of correlation, there is no point in using them both (or all). These features become dimensionally redundant. In that case, we drop features and save computation time. Principal component analysis (PCA) becomes extremely useful in such cases when features are linearly (or even monotonically) related to each other. Using PCA, the number of features reduced to 200 from 301 original features (i.e., frequency points) in $S_{11}$ data. This reduces high-dimensional complexity, without losing the patterns in the dataset, i.e., features with maximum variance.

## VI. RESULTS AND DISCUSSION

Recently, many researchers have used machine learning models for automatic impedance matching [36], [37], [38]. However, their applications are either limited to WPT with low frequency operation (few MHz) or based on complex neural networks with several dense layers. The proposed model learns from simulated magnitude values of input reflection coefficients instead of measuring complex impedances with expensive network analyzer. Fig. 6(a)-(b) show the actual (true values) and the predicted values of parallel capacitor and series inductor, respectively. To understand the stability of

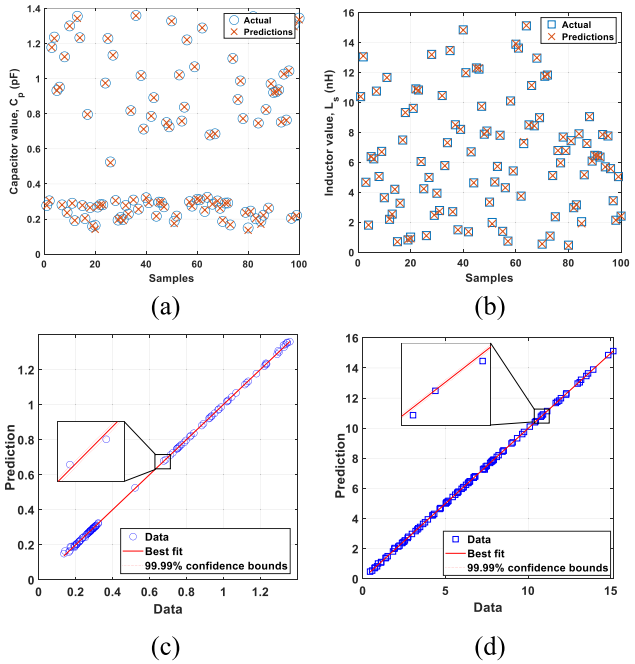


**FIGURE 6.** (a) Actual vs predicted values of (a) parallel capacitor, $C_P$ (b) series inductor, $L_S$; Observation data vs models best fit for (c) parallel capacitor (d) series inductor.

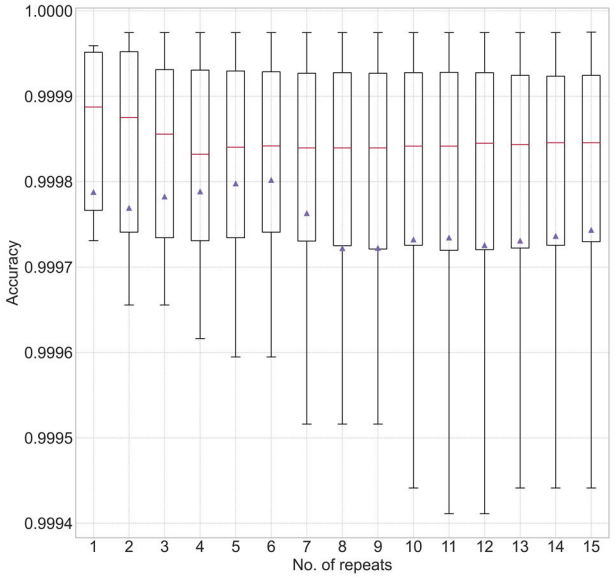


**FIGURE 7.** Summary of a repeated 10-fold cross validation with 15 repeats.

**TABLE 3.** Validation of the proposed SLM Based AIM.

| Sample No. | Calculated tuning parameters | | Predicted tuning parameters | | | |
|---|---|---|---|---|---|---|
| | $C_p$ (fF) | $L_s$ (nH) | $\hat{C}_p$ (fF) | Pred. Error | $\hat{L}_s$ (nH) | Pred. Error |
| 03 | 1177.57 | 4.68 | 1177.930633 | 0.01% | 4.68303888 | 0.10% |
| 27 | 1133.73 | 5.00 | 1133.890469 | 0.01% | 5.01453847 | 0.30% |
| 99 | 220.60 | 5.06 | 219.9955998 | 0.27% | 5.04985205 | 0.11% |
| 53 | 1021.24 | 5.74 | 1020.897274 | 0.03% | 5.74099386 | 0.08% |
| 76 | 881.24 | 6.80 | 882.0455576 | 0.09% | 6.79479015 | 0.02% |

prediction accuracy, confidence bounds are given in Fig. 6(c)-(d) along with model's regression lines to fit the data points. Confidence bounds create a space between two lines that shows uncertainty around mean predictions. So, a 99.99% confidence bounds means that there is a 99.99% probability that the model's true best-fit regression line (solid line) lies within the confidence interval (dotted line) of the regression line calculated from the data points. To quantify the prediction accuracy of the proposed model, we performed repeated $k$-fold cross validation. A $k$-fold cross-validation effectively estimates the model's predictive performance; however, the performance can vary each time for different splits. To avoid this, we performed repeated $k$-fold cross-validation by repeating the regular cross validation process several times and taking mean of results each time.

A summary of 10-fold cross validation with 15 repeats is shown in Fig. 7. The accuracy fluctuates approximately at 0.99980 during the first 4 repeats. However, it remains constant at 0.999850 from5th repeat onwards. This can be considered as a stable performance indicator of prediction accuracy of the proposed model. Higher accuracies are extremely desirable while determining the tuning parameters as it greatly determines RL, reflection coefficient, mismatch-loss and reflected power. Here, the RL becomes a useful way to measure power loss (mostly) due to the impedance mismatch. It is a measure of all the reflections that are caused by the impedance mismatches. It is calculated as the ratio of the power in the rejected travelling wave to the power in the incident wave. A higher RL is always desirable as it indicates that less power is reflected from the antenna. Similarly, a lower RL implies more power is reflected from the load due to impedance mismatch. VSWR and reflection coefficients in (7) and (8) are also used to measure RL. Further, we calculate the mismatch loss (in dB) as $-10\left[\log\left[1-|\Gamma|^2\right]\right]$, and the reflected power in percentage as $100\left|\Gamma^2\right|$.

For validation, we considered 6 sets of calculated tuning parameters using (12) and (13), mentioned as 'Calculated tuning parameters' in Table 3. Then, corresponding $S_{11}$ data from the validation dataset was applied to the SLM to predict the tuning parameters. We calculated prediction errors for both parameters for further analysis in this section. Next, Table 4 shows the impact of the prediction error on mismatch loss and transmitted (and reflected) power. We have sorted the test samples according to the descending order of the reflection coefficient to consider most of the worst cases (high prediction error). Results show that for the highest $\Gamma = 0.098$ (sample no. 20), with 13.83% and 9.86% prediction errors of tuning parameters, respectively, the proposed SLM ensures RL = -20.18 dB with ≈1% reflected power. This is the highest amount of reflected power due to the prediction error with the proposed SLM. During practical implementation of the proposed solution other losses such as the losses due to the measurement may also arise. Generally, the frequency

**TABLE 4.** The impact of the prediction error on return loss, mismatch loss and power transfer.

| Sample No. | Calculated tuning parameters | | Predicted tuning parameters | | Prediction error in % | | Simulated $\|S_{11}\|$ (in dB) with | | Reflection coefficient ($\Gamma$) ↓* | Mismatch loss | Transmitted power | Reflected power |
|---|---|---|---|---|---|---|---|---|---|---|---|---|
| | $C_p$ (fF) | $L_s$ (nH) | $\hat{C}_p$ (fF) | $\hat{L}_s$ (nH) | (for $C_p$) | (for $L_s$) | calculated parameters | predicted parameters | | (dB) | (%) | (%) |
| 20 | 164.368 | 1.017 | 141.637 | 0.916 | 13.829 | 9.855 | -48.362 | -20.181 | 0.098 | 0.0419 | 99.041 | 0.959 |
| 26 | 525.521 | 1.116 | 521.034 | 1.109 | 0.854 | 0.637 | -24.653 | -20.978 | 0.089 | 0.0348 | 99.202 | 0.798 |
| 42 | 784.986 | 1.371 | 787.612 | 1.375 | 0.335 | 0.268 | -22.345 | -20.999 | 0.089 | 0.0346 | 99.206 | 0.794 |
| 55 | 837.531 | 1.402 | 839.185 | 1.398 | 0.197 | 0.237 | -22.646 | -21.662 | 0.083 | 0.0297 | 99.318 | 0.682 |
| 80 | 149.508 | 0.479 | 136.165 | 0.437 | 8.925 | 8.729 | -56.061 | -22.909 | 0.072 | 0.0223 | 99.488 | 0.512 |
| 57 | 299.316 | 0.751 | 297.449 | 0.736 | 0.624 | 1.938 | -31.748 | -23.616 | 0.066 | 0.0189 | 99.565 | 0.435 |
| 51 | 187.618 | 1.993 | 175.175 | 1.906 | 6.632 | 4.338 | -46.251 | -24.485 | 0.060 | 0.0155 | 99.644 | 0.356 |
| 19 | 158.420 | 0.829 | 163.130 | 0.859 | 2.973 | 3.556 | -37.474 | -25.009 | 0.056 | 0.0137 | 99.684 | 0.316 |
| 31 | 197.859 | 2.791 | 191.970 | 2.742 | 2.976 | 1.741 | -48.050 | -25.385 | 0.054 | 0.0126 | 99.711 | 0.289 |
| 63 | 243.142 | 7.259 | 251.650 | 7.374 | 3.499 | 1.579 | -52.706 | -25.943 | 0.050 | 0.0111 | 99.745 | 0.255 |
| 85 | 188.420 | 2.045 | 170.843 | 1.924 | 9.328 | 5.942 | -49.552 | -26.115 | 0.049 | 0.0106 | 99.755 | 0.245 |
| 38 | 1017.941 | 1.503 | 1017.538 | 1.500 | 0.040 | 0.213 | -27.416 | -26.724 | 0.046 | 0.0092 | 99.787 | 0.213 |
| 73 | 166.408 | 1.083 | 168.150 | 1.098 | 1.047 | 1.394 | -37.746 | -28.532 | 0.037 | 0.0061 | 99.860 | 0.140 |
| 61 | 309.706 | 13.637 | 309.229 | 13.620 | 0.154 | 0.127 | -30.049 | -29.204 | 0.035 | 0.0052 | 99.880 | 0.120 |
| 9 | 237.811 | 6.740 | 235.595 | 6.711 | 0.932 | 0.428 | -34.007 | -29.383 | 0.034 | 0.0050 | 99.885 | 0.115 |
| 15 | 276.931 | 0.711 | 278.316 | 0.707 | 0.500 | 0.667 | -33.373 | -29.476 | 0.034 | 0.0049 | 99.887 | 0.113 |
| 22 | 282.319 | 10.912 | 281.696 | 10.894 | 0.221 | 0.161 | -30.843 | -29.666 | 0.033 | 0.0047 | 99.892 | 0.108 |
| 29 | 194.167 | 2.470 | 196.967 | 2.491 | 1.442 | 0.874 | -38.693 | -29.731 | 0.033 | 0.0046 | 99.894 | 0.106 |
| 28 | 305.567 | 13.215 | 305.069 | 13.198 | 0.163 | 0.132 | -30.660 | -29.754 | 0.033 | 0.0046 | 99.894 | 0.106 |
| ⋮ | ⋮ | ⋮ | ⋮ | ⋮ | ⋮ | ⋮ | ⋮ | ⋮ | ⋮ | ⋮ | ⋮ | ⋮ |
| 53 | 1021.245 | 5.736 | 1020.897 | 5.741 | 0.034 | 0.078 | -47.513 | -46.979 | 0.004 | 0.0001 | 99.998 | 0.002 |
| 76 | 881.236 | 6.796 | 882.046 | 6.795 | 0.092 | 0.023 | -47.847 | -47.298 | 0.004 | 0.0001 | 99.998 | 0.002 |
| 99 | 220.601 | 5.055 | 219.996 | 5.050 | 0.274 | 0.106 | -50.884 | -48.949 | 0.004 | 0.0001 | 99.999 | 0.001 |
| 92 | 936.246 | 6.360 | 936.288 | 6.361 | 0.004 | 0.029 | -52.798 | -52.623 | 0.002 | 0.0000 | 99.999 | 0.001 |

* Samples are sorted in descending order of the reflection coefficient to show most of the worst cases.

domain-based measurements are highly accurate and have much lower noise compared to the time domain-based measurements. Measurement losses of approximately 0.3 dB to 0.5 dB are expected while using directional couplers. However, measurement losses are functions of the directivity of the device and can be very negligible for highly directive coupler.

To illustrate the impact of prediction error mentioned in Table 3 and Table 4, we simulated the inverted-F antenna with newly predicted $C_p$ and $L_s$. In Fig. 8, we compared the simulated $S_{11}$ results using predicted tuning parameters (shown in dashed lines) with calculated tuning parameters (shown in solid lines). Results confirm similar performances when compared between the two. The figure also shows that the proposed AIM circuit tuned by SLM can dynamically track any shifts in the resonance frequency over a wide range of frequency from 2 to 3 GHz without changing the operational 10-dB bandwidth (200 MHz). The maximum reflection coefficients were −23.5 dB at 2.5 GHz. A single inverted-F antenna was used during modelling and simulation. This concept can also be adopted to multiple antenna systems (including base stations) equipped with array of

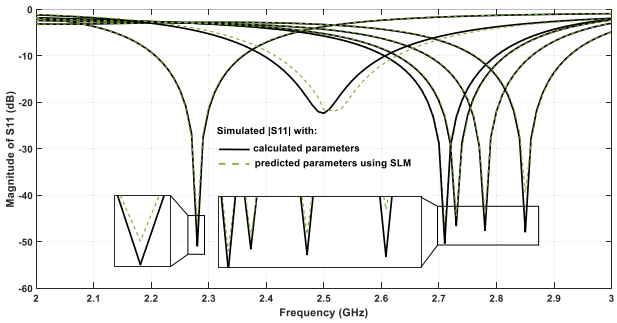


**FIGURE 8.** Simulated magnitude of $S_{11}$ using impedance matching with tuning parameters obtained by proposed SLM (shown in dash-lines) and compared with mathematically obtained tuning parameters (shown in solid lines) and the dataset for 6 samples.

antennas. However, multiple antenna system creates mutual coupling among the closely spaced antenna elements and significantly influences radiation pattern, reduces transmission capacity, and changes input impedance. This can be addressed by using a decoupling network to isolate the effect of mutual coupling. The automatic impedance matching

technique presented in this work using SLM is validated through simulation only. However, it can be practically implemented using a control module including the proposed SLM and a network of tuneable inductors and capacitors (our future work).

Ridge estimation can be computed efficiently using singular value decomposition. If the dataset is represented as a data-matrix of shape $N \times C$, then the computational cost of the ridge estimation has a cost of $O(NC^2)$ where $N$ is the number of sample (data size), and $C$ is the number of input feature (feature size). On the other hand, machine learning based previous works in antenna impedance matching used neural networks [34], [35], [36], [37], [38]. The computational complexity to train a neural network depends on many factors, such as the number of iterations, number of hidden layers, and the number of neurons in each layer, size of the dataset, etc. There are, however, many frameworks available to compute complex structures of deep neural networks efficiently such as TensorFlow, Keras, PyTorch, etc. In general, the computation complexity of a neural network-based solution is $O(NCn_l n_i)$, where $n_l$ is the number of hidden layers and $n_i$ is the number of iterations. Here, the computational complexity will greatly depend on the number of iterations and data size. For example, the previous neural network-based work for AIM takes approximately 10.5 minutes for training [38] using Intel(R) processor at 2.30GHz and 16GB memory, whereas the proposed SLM took 0.05 seconds for the training using same processor at 2.50GHz and 32GB memory.

It is possible to determine the matching circuit parameter values analytically. However, this would require the complex impedances (both magnitude and phase) or reflection coefficients of the antenna. These can be measured using time domain-based reflectometer, or a frequency domain-based vector network analyser or spectrum analyser. The proposed technique in this work can tune over a wide range of frequency band from 2 to 3GHz. Collecting complex measurements over such a wide frequency range, in the laboratory environment, using vector network analyser would be time consuming and cumbersome. Assuming we have the complex measurements, we would still need to use (12) and (13) to compute the circuit parameters. It is clear from the equations that solving them would require several complex additions, complex multiplications, division of complex conjugates, squaring complex terms, and then finding root-mean-square of complex terms in quadratic equation. So, computing the circuit parameters analytically (and frequently) would be computationally expensive for battery operated mobile devices. Our proposed model, on the other hand, requires 0.05 seconds (50ms) for the training, and a trained model takes only 0.001 second (1ms) to make a prediction which can automatically tune itself. This quick predictability makes the proposed technique more suitable for real-time applications than analytical computations.

A comparison of the proposed model with other machine learning based solutions for impedance matching is given in Table 5. The impedance matching techniques proposed in [36] and [37] are applicable for the applications related to WPT and cannot tune antenna impedances. Moreover, the operating frequencies are not suitable for mobile communication. Although the DNN based algorithm proposed in [38] can construct impedance matching circuits for mobile communication but the algorithm requires 10.5 minutes using Intel(R) Xenon(R) processor at 2.30 GHz and 16 GB memory. This time complexity restricts its use for many real-time applications. On the other hand, the proposed model in this work requires only 1ms to make a prediction, where one prediction provides both the values of tuning parameters for the AIM circuit.

**TABLE 5. Comparison of reported machine learning models for impedance matching.**

| Ref. | AIM circuit type | Application | Freq. | Learning method | Network size | Algorithm speed | Prediction accuracy |
|---|---|---|---|---|---|---|---|
| [36] | L-type-three stages | WPT | 13.56 MHz | Neural network | 12 layers (10 hidden layers) | ≈ 0.063 sec. | 90.00% |
| [37] | Gamma network | WPT | 6.78 MHz | Neural network | 5 layers (3 hidden layers) | ≈ 0.063 sec. | 99.00% |
| [38] | Gamma network | Antenna | 0.9 to 1.4 GHz | Neural network | 12 layers (10 hidden layers) | ≈ 10.5 min. | 99.90% |
| This work | A single L-type | Antenna | 2 to 3 GHz | Shallow learning | No hidden layers | ≈ 0.05 sec. | 99.985% |

## VII. CONCLUSION

The resonance frequency of an antenna can be affected by user proximity, presence of the human body (or body parts), nearby objects, or other environmental factors causing impedance mismatch in the RF front-end and other sensitive applications such antenna sensors. A poorly matched antenna-transceiver section causes severe power loss, reduces transmission range and overall performance. An impedance matching circuit can mitigate this by quickly responding to the rapid fluctuations in the antenna's operational conditions. A fast, effective, and low-complexity solution has always been a challenge for this purpose. We proposed, for the first time, a low-complexity shallow learning-based model to construct impedance matching circuit. We designed a novel inverted-F antenna to evaluate and validate the performances of impedance matching circuits. We calculated several true values of the impedance matching circuit parameter and created 500 interpolation points. Using these points, we simulated the antenna with impedance matching and generated $S_{11}$ dataset. Then, 400 samples are used to train the proposed model and 100 are used for the validation. We addressed multicollinearities in the dataset, and yet used that to our advantage and improved model's accuracy. We used dimensionality reduction technique using PCA to avoid high-dimensional complexity at the same time. For validation, the proposed antenna is simulated using the calculated (theoretical) and predicted tuning parameters and matching performances are compared. Results show negligible differences in terms of

resonance frequency, reflection coefficients, and operational bandwidth. A summary of 10-fold cross validation with 15 repeats confirms that the proposed SLM has 0.99985 predictive accuracy. The impact of the prediction error on return loss, mismatch loss and power transmission are also discussed. Results show that with the highest prediction errors of 13.83% and 9.86% for the tuning parameters, respectively, the proposed SLM ensures RL = -20.18 dB with $\approx$ 1% reflected power. This is the highest amount of reflected power due to the model's prediction error. The proposed low-complexity model requires 0.05 seconds for the training and 0.001 seconds for prediction making it suitable for wireless application in terms of speed and accuracy. The technique can be expanded for other antenna types as well as for multiple antenna systems utilizing a network of tuneable inductors and capacitors.

## REFERENCES

[1] K. R. Boyle, Y. Yuan, and L. P. Ligthart, "Analysis of mobile phone antenna impedance variations with user proximity," *IEEE Trans. Antennas Propag.*, vol. 55, no. 2, pp. 364–372, Feb. 2007.

[2] B. Couraud, R. Vauche, S. N. Daskalakis, D. Flynn, T. Deleruyelle, E. Kussener, and S. Assimonis, "Internet of Things: A review on theory based impedance matching techniques for energy efficient RF systems," *J. Low Power Electron. Appl.*, vol. 11, no. 2, p. 16, Mar. 2021.

[3] M. I. Hossain, M. R. I. Faruque, and M. T. Islam, "Investigation of hand impact on PIFA performances and SAR in human head," *J. Appl. Res. Technol.*, vol. 13, no. 4, pp. 447–453, Aug. 2015.

[4] G. Sacco, D. Nikolayev, R. Sauleau, and M. Zhadobov, "Antenna/human body coupling in 5G millimeter-wave bands: Do age and clothing matter?" *IEEE J. Microw.*, vol. 1, no. 2, pp. 593–600, Apr. 2021.

[5] J. W. Adams, L. Chen, P. Serano, A. Nazarian, R. Ludwig, and S. N. Makaroff, "Miniaturized dual antiphase patch antenna radiating into the human body at 2.4 GHz," *IEEE J. Electromagn., RF Microw. Med. Biol.*, vol. 7, no. 2, pp. 182–186, Jun. 2023.

[6] U. Ali, S. Ullah, B. Kamal, L. Matekovits, and A. Altaf, "Design, analysis and applications of wearable antennas: A review," *IEEE Access*, vol. 11, pp. 14458–14486, 2023.

[7] M. Ziane, R. Sauleau, and M. Zhadobov, "Antenna/body coupling in the near-field at 60 GHz: Impact on the absorbed power density," *Appl. Sci.*, vol. 10, no. 21, p. 7392, Oct. 2020.

[8] T. Alam and M. Cheffena, "Integrated microwave antenna/sensor for sensing and communication applications," *IEEE Trans. Microw. Theory Techn.*, vol. 70, no. 11, pp. 5289–5300, Nov. 2022.

[9] T. Alam, M. Cheffena, and E. Rajo-Iglesias, "Dual-functional communication and sensing antenna system," *Sci. Rep.*, vol. 12, no. 1, p. 20387, Nov. 2022.

[10] R. Kozak, K. Khorsand, T. Zarifi, K. Golovin, and M. H. Zarifi, "Patch antenna sensor for wireless ice and frost detection," *Sci. Rep.*, vol. 11, no. 1, p. 13707, Jul. 2021.

[11] R. U. Tariq, M. Ye, X.-L. Zhao, S.-C. Zhang, Z. Cao, and Y.-N. He, "Microwave sensor for detection of ice accretion on base station antenna radome," *IEEE Sensors J.*, vol. 21, no. 17, pp. 18733–18741, Sep. 2021.

[12] M. El Gharbi, R. Fernández-García, S. Ahyoud, and I. Gil, "A review of flexible wearable antenna sensors: Design, fabrication methods, and applications," *Materials*, vol. 13, no. 17, p. 3781, Aug. 2020.

[13] X. Jin, S. Liu, Y. Yang, and Y. Zhou, "A frequency-reconfigurable planar slot antenna using S-PIN diode," *IEEE Antennas Wireless Propag. Lett.*, vol. 21, no. 5, pp. 1007–1011, May 2022.

[14] T. K. Nguyen, C. D. Bui, A. Narbudowicz, and N. Nguyen-Trong, "Frequency-reconfigurable antenna with wide- and narrowband modes for sub-6 GHz cognitive radio," *IEEE Antennas Wireless Propag. Lett.*, vol. 22, no. 1, pp. 64–68, Jan. 2023.

[15] K. Paramayudha, S. J. Chen, W. Withayachumnankul, and C. Fumeaux, "Frequency-reconfigurable circularly polarized omnidirectional antenna," *IEEE Trans. Antennas Propag.*, vol. 70, no. 8, pp. 7205–7210, Aug. 2022.

[16] S. Subbaraj, M. Kanagasabai, M. G. N. Alsath, S. K. Palaniswamy, S. Kingsly, I. Kulandhaisamy, A. K. Shrivastav, R. Natarajan, and S. Meiyalagan, "A compact frequency-reconfigurable antenna with independent tuning for hand-held wireless devices," *IEEE Trans. Antennas Propag.*, vol. 68, no. 2, pp. 1151–1154, Feb. 2020.

[17] S. Wang, F. Fan, F. Zhang, Y. Li, G. Zhang, S.-W. Wong, and L. Zhu, "A frequency-reconfigurable inverted-L antenna made of pure water," *IEEE Antennas Wireless Propag. Lett.*, vol. 21, no. 1, pp. 109–113, Jan. 2022.

[18] S. N. M. Zainarry, S. J. Chen, and C. Fumeaux, "A frequency-reconfigurable single-feed zero-scanning antenna," *IEEE Trans. Antennas Propag.*, vol. 71, no. 2, pp. 1359–1368, Feb. 2023.

[19] N. O. Parchin, H. J. Basherlou, Y. I. A. Al-Yasir, A. M. Abdulkhaleq, and R. A. Abd-Alhameed, "Reconfigurable antennas: Switching techniques—A survey," *Electronics*, vol. 9, no. 2, p. 336, Feb. 2020.

[20] A. van Bezooijen, M. A. de Jongh, F. van Straten, R. Mahmoudi, and A. van Roermund, "Adaptive impedance-matching techniques for controlling *L* networks," *IEEE Trans. Circuits Syst. I, Reg. Papers*, vol. 57, no. 2, pp. 495–505, Feb. 2010.

[21] E. L. Firrao, A.-J. Annema, and B. Nauta, "An automatic antenna tuning system using only RF signal amplitudes," *IEEE Trans. Circuits Syst. II, Exp. Briefs*, vol. 55, no. 9, pp. 833–837, Sep. 2008.

[22] M. Huang, Y. Lu, Q.-A. Zhu, M. Salek, Y. Wang, J. Huang, and T. Liu, "Highly integrated PA-PIFA with a wide frequency tuning range," *IEEE Antennas Wireless Propag. Lett.*, vol. 20, no. 8, pp. 1433–1437, Aug. 2021.

[23] I. Vasilev, V. Plicanic, and B. K. Lau, "Impact of antenna design on MIMO performance for compact terminals with adaptive impedance matching," *IEEE Trans. Antennas Propag.*, vol. 64, no. 4, pp. 1454–1465, Apr. 2016.

[24] M. Alibakhshikenari, B. S. Virdee, L. Azpilicueta, C. H. See, R. Abd-Alhameed, A. A. Althuwayb, F. Falcone, I. Huynen, T. A. Denidni, and E. Limiti, "Optimum power transfer in RF front end systems using adaptive impedance matching technique," *Sci. Rep.*, vol. 11, no. 1, p. 11825, Jun. 2021.

[25] Y. Sun, J. Moritz, and X. Zhu, "Adaptive impedance matching and antenna tuning for green software-defined and cognitive radio," in *Proc. IEEE 54th Int. Midwest Symp. Circuits Syst. (MWSCAS)*, Aug. 2011, pp. 1–4.

[26] Y. Sun, "Antenna impedance matching using genetic algorithms," in *Proc. IEE Nat. Conf. Antennas Propag.*, Aug. 1999, pp. 31–36.

[27] A. X. Chen, T. H. Jiang, Z. Z. Chen, and Y. Zhang, "A genetic and simulated annealing combined algorithm for optimization of wideband antenna matching networks," *Int. J. Antennas Propag.*, vol. 2012, Apr. 2012, Art. no. 251624.

[28] Y. Tan, Y. Sun, and D. Lauder, "Automatic impedance matching and antenna tuning using quantum genetic algorithms for wireless and mobile communications," *IET Microw., Antennas Propag.*, vol. 7, no. 8, pp. 693–700, Jun. 2013.

[29] M. Alibakhshikenari, B. S. Virdee, P. Shukla, C. H. See, R. A. Abd-Alhameed, F. Falcone, and E. Limiti, "Improved adaptive impedance matching for RF front-end systems of wireless transceivers," *Sci. Rep.*, vol. 10, no. 1, p. 14065, Aug. 2020.

[30] J. Bito, S. Jeong, and M. M. Tentzeris, "A real-time electrically controlled active matching circuit utilizing genetic algorithms for wireless power transfer to biomedical implants," *IEEE Trans. Microw. Theory Techn.*, vol. 64, no. 2, pp. 365–374, Feb. 2016.

[31] Y. Li, W. Dong, Q. Yang, S. Jiang, X. Ni, and J. Liu, "Automatic impedance matching method with adaptive network based fuzzy inference system for WPT," *IEEE Trans. Ind. Informat.*, vol. 16, no. 2, pp. 1076–1085, Feb. 2020.

[32] H. Song, S.-H. Oh, J. T. Aberle, B. Bakkaloglu, and C. Chakrabarti, "Automatic antenna tuning unit for software-defined and cognitive radio," in *IEEE Antennas Propag. Soc. Int. Symp. Dig.*, Jun. 2007, pp. 85–88.

[33] M. Alibakhshikenari, B. S. Virdee, C. H. See, R. A. Abd-Alhameed, F. Falcone, and E. Limiti, "Automated reconfigurable antenna impedance for optimum power transfer," in *Proc. IEEE Asia–Pacific Microw. Conf. (APMC)*, Dec. 2019, pp. 1461–1463.

[34] F. Mir, L. Kouhalvandi, and L. Matekovits, "Deep neural learning based optimization for automated high performance antenna designs," *Sci. Rep.*, vol. 12, no. 1, p. 16801, Oct. 2022.

[35] J. Choo, T. H. A. Pho, and Y.-H. Kim, "Machine learning technique to improve an impedance matching characteristic of a bent monopole antenna," *Appl. Sci.*, vol. 11, no. 22, p. 10829, Nov. 2021.

[36] Y. Li, W. Dong, Q. Yang, J. Zhao, L. Liu, and S. Feng, "An automatic impedance matching method based on the feedforward-backpropagation neural network for a WPT system," *IEEE Trans. Ind. Electron.*, vol. 66, no. 5, pp. 3963–3972, May 2019.
[37] S. Jeong, T.-H. Lin, and M. M. Tentzeris, "A real-time range-adaptive impedance matching utilizing a machine learning strategy based on neural networks for wireless power transfer systems," *IEEE Trans. Microw. Theory Techn.*, vol. 67, no. 12, pp. 5340–5347, Dec. 2019.
[38] J. H. Kim and J. Bang, "Antenna impedance matching using deep learning," *Sensors*, vol. 21, no. 20, p. 6766, Oct. 2021.
[39] F. N. Fritsch and J. Butland, "A method for constructing local monotone piecewise cubic interpolants," *SIAM J. Sci. Comput.*, vol. 5, no. 2, pp. 300–304, 1984.
[40] C. B. Moler, "Interpolation," in *Numerical Computing With MATLAB*. Philadelphia, PA, USA: SIAM, 2004, pp. 99–100.

**MOHAMMAD MAHMUDUL HASAN** received the B.Tech. and M.Tech. degrees in electronics and telecommunication engineering from KIIT University, India. He is currently pursuing the Ph.D. degree in information and communication technology with from the Norwegian University of Science and Technology (NTNU), Norway. In 2010, he was an Assistant Professor with KIIT University. From 2011 to 2022, he was an Assistant Professor with the Department of Electronics and Communication Engineering, UITS, Bangladesh. He has written and/or edited several journals and conference papers. His research interests include wireless communications, signal processing, machine learning and intelligent systems, antenna engineering, antenna sensors, massive MIMO, and millimeter wave communications.

**MICHAEL CHEFFENA** received the M.Sc. degree in electronics and computer technology from the University of Oslo, Norway, in 2005, and the Ph.D. degree from the Norwegian University of Science and Technology (NTNU), Trondheim, Norway, in 2008. In 2007, he was a Visiting Researcher with the Communications Research Centre, Ottawa, ON, Canada. From 2009 to 2010, he conducted a Postdoctoral Researcher with the University Graduate Center, Kjeller, Norway; and with the French Space Agency, Toulouse, France. He is currently a Full Professor with NTNU, Gjøvik, Norway. His research interests include the modeling and prediction of propagation radio channels, signal processing, medium access control protocol design, antenna sensors, and sensor systems.